Energy & Buildings 214 (2020) 109815

Contents lists available at ScienceDirect

Energy & Buildings

journal homepage: www.elsevier.com/locate/enbuild

Investigation on the thermal performance of a composite Trombe wall under steady state condition

Liqun Zhou[a,*], Junpeng Huo[b], Tong Zhou[c], Shufeng Jin[a]

[a] College of Petrochemical Technology, Lanzhou University of Technology, Lanzhou 730050, China
[b] Department of Mechanical Engineering, University of Alberta, Alberta T6R1Y2, Canada
[c] Gansu Urban & Rural Planning Design Institute Co. Ltd, Lanzhou 730030, China

ARTICLE INFO

Article history:
Received 22 September 2019
Revised 17 January 2020
Accepted 23 January 2020
Available online 14 February 2020

Keywords:
Trombe wall
Water wall
Low-temperature water
Energy analysis
Exergy analysis
Heat loss

ABSTRACT

A composite Trombe wall is proposed which combines the water wall with the traditional Trombe wall. Computational fluid dynamics models for different types of Trombe walls were developed to investigate the flow and thermal performance. A good agreement was achieved between simulation results and relevant literature's data. The result shows that the Water Trombe wall could achieve best thermal performance. It can improve the operating efficiency during daytime. The thermal efficiency of the Water Trombe wall is 3.3% higher than the traditional Trombe wall at certain conditions. At nighttime, this structure has the advantage to directly utilize low-temperature water for decreasing building's heat loss. Under low irradiation conditions, the efficiency is 7.2% higher than the traditional Trombe wall. In simulated conditions, the results indicate that the Water Trombe wall can reduce heat loss by 31% compared with the traditional Trombe wall at night. The influence of temperature and velocity of low-temperature water was studied. The mass flow rate of water has minor effect on thermal performance of the Water Trombe wall.

Abbreviations

TW	Trombe wall
WTW	Water Trombe wall
GWTW	Glass-Water Trombe wall
CFD	Computational Fluid Dynamics
DO	Discrete Ordinates
SST	Shear Stress Transfer
PCM	Phase change material
PV	Photovoltaic
PC	Polycarbonate
RE	Relative error

1. Introduction

According to the statistics, the energy consumption for space heating was reached up to 131.3 million tce in China's rural area, which is accounting for 41.5% of total rural energy consumption [1]. The source of main primary energy is coal and straw in these regions. However, due to the oxygen deficient at high altitudes, incomplete combustion of fossil fuels may cause environmental pollution and troubles in ecological cycles. In this situation, there is an urgent need to seek solutions to reduce the energy consumption of residential space heating without affecting the comfort of the indoor temperatures in the winter. Combining the passive solar systems with buildings can effectively reduce the consumption of non-renewable energy to achieve the goal of sustainable development, which has attracted the attention of the scholars and encouraged by international regulations [2]. In order to provide heat for a house without power and fossil energy consumption, some solar thermal energy conversion systems, for instance, solar chimneys, solar water systems, solar roofs and Trombe walls, were designed and manufactured [3].

Passive solar heating such as Trombe wall (TW) is widely used in cold climates. The Trombe wall is a classic passive solar technology that has a wide range of attention due to its simple structure, good thermal performance and low operating cost. However, the TW still has some drawbacks that limits its promotion and using [4]. Most of all, in nighttime and shaded daytime of the winter, a large amount of heat is transferred from the indoor through the TW to the outside, causing extra energy consumption. Improvements were developed for the purpose of overcoming the problem [5]. Bajc et al. [6] built a three-dimensional numerical model to analyze the temperature fields of the Trombe wall for a moderate continental climate. The structure of Trombe wall was optimized

* Corresponding author.
E-mail address: zhoulq@lut.edu.cn (L. Zhou).

https://doi.org/10.1016/j.enbuild.2020.109815
0378-7788/

Nomenclature

A_{wall}	effective solar absorbing area, m^2
I	solar radiation, W/m^2
Q_{air}	heat transfer flux in air channel, W/m^2
Q_{loss}	heat loss to the outside, W/m^2
Ex	exergy, W/m
μ	viscosity, kg/(m s)
h	heat transfer coefficient, $W/(m^2\ ^\circ C)$
T	temperature, °C
T_{out}	temperature of upper vent, °C
g	gravitational acceleration, m/s^2
η_{ex}	exergy efficiency
c_p	specific heat at constant pressure, J/(kg °C)
η	thermal efficiency
$\dot{m}$	mass flow rate, kg/s

Subscripts

a	ambient
in	lower vent
out	upper vent
s	sun
rad	radiation

by CFD simulation method. Hong et al. [7] proposed an improved Trombe wall, which equipped with a venetian blind. The flow and heat transfer characteristics were studied based on CFD simulation. The influence of the location of the venetian blind on solar thermal efficiency was achieved. The optimization of the width of air duct and the area of inlet and outlet vents were discussed in detail. Dong et al. [8] designed an improved Trombe wall in Harbin, China, of which the absorber plate was installed between the glass cover and thermal storage wall instead of pasting on the thermal storage wall. The result indicated that the thermal efficiency of the novel Trombe wall is 50% higher, compared with that of the TW during the daytime at Harbin, China. Abbassi et al. [9] proposed a Trombe wall containing internal thermal fins. The conclusion indicated that the insertion of the thermal fins was benefit to an increase of the indoor temperature and a decrease of the heat transfer from the room to outdoor. Koyunbaba et al. [10] carried out the comparison of single glass, double glass and a semitransparent PV module integrated on the Trombe wall in Izmir, Turkey through experiments. Saadatian et al. [11] reviewed the application of Trombe walls in buildings and discussed the characteristics of Trombe walls, including Trombe wall configurations, and Trombe wall technology.

Compared with traditional construction materials, phase change material (PCM) can provide a higher thermal capacity by its latent heat of fusion. Therefore, the PCM has been widely applied in buildings. Kara et al. [12] evaluated the thermal behavior of the Trombe wall that combined with novel triple glass and PCM in Erzurum, Turkey. The experiment showed that the new Trombe wall could provide 14 percent of the annual heat load for the test building. Liu et al. [13] investigated thermal properties of a new ventilated Trombe wall integrated with PCM. The influence of the airflow rate, the optical property of solar coating was conducted. The obtained result showed that melting temperature 22 °C for interior PCM and the latent heat 176 kJ/kg for exterior PCM performed at optimum operating level under the weather condition in Changsha, China. The integration of photovoltaic (PV) with the Trombe wall is a novel version [14]. The PV-Trombe wall is a new multi-functional structure that combines the traditional building heating structure Trombe wall with solar photovoltaic cells. It can realize the function of heating and ventilation while providing electricity for production and life. Hu et al. [15] developed a novel PV blind-integrated Trombe wall module. The impact of different inlet air flow rates and PV blind angles on photoelectric conversion efficiency and heat gains of the module is measured and analyzed.

Water wall is an effective solution for maintaining the thermal comfort of buildings and reducing energy consumption [16,17]. In winter, water wall could absorb solar radiation and store heat during the sunny day, while releasing it to the room at night to reduce the building's heating load. The cost of water wall is also significantly lower than the cost of a massive wall using phase change materials [18]. Considering the temperature of building envelopes is significantly colder than that of indoor spaces, it is very promising to use low-grade natural energy for heating in winter [19]. For instance, when the outdoor temperature is low in winter, low-grade thermal water could be used naturally with a temperature between the room air temperature and the outdoor air temperature, which can be potentially worked to either counterbalance the thermal load or indirectly heat the space [20]. And, the low-grade energy sources may be ground water, natural water, solar water heating system and geothermal energy produced by the ground-coupled heat exchanger system. With the proposed approach, the water wall can be considered as thermal active building envelope.

In this study, a composite Trombe wall is proposed, which integrates the traditional Trombe wall with the water wall as the building envelope. The thermal performance of the composite Trombe wall is studied by computational fluid dynamics (CFD) method. The exergy and energy performances of traditional and composite Trombe wall are evaluated by the simulated data. The ability of the composite Trombe wall utilizing the low-temperature water for heat preservation is investigated at night. Based on the analysis of the energy saving potential and economic efficiency, the influence of inlet velocity and water temperature is optimized.

2. Description of the composite Trombe wall

The two designed structures of composite Trombe walls are shown in Fig. 1. The first is Glass-Water Trombe wall (GWTW), which add a water wall between the glass cover and the massive wall. The other is Water Trombe wall (WTW), which set the water wall as the outside layer directly. It should be mentioned that only the structure between the glass cover and the massive wall is considered in present study. The water wall comprises a PC cavity filled with water. The PC cavity is made semi-transparent PC sheets. Special attention has been paid to the water tightness of the PC cavity by using a number of screws and silicone to prevent water leakage.

Fig. 2 shows the operation mode of the composite Trombe wall systems during day and night, respectively. On sunny days, visible and near-infrared spectrum can pass through the water wall, then the coating on massive wall converts the solar energy into heat. Meanwhile, the far-infrared spectrum is absorbed by the water, leading a temperature rise in water wall. The overall temperature of the air flow channel rises that preventing the hot air from shrinking on the cold wall surface, and an anti-siphon phenomenon occurs (the "reverse flow" occurs in the flow channel). At night, low-temperature water can be circuited in the water layer to reduce the heat loss of the composite Trombe wall.

3. Energy and exergy analysis

The energy and exergy analysis were adapted to evaluate the thermal performance of the composite Trombe wall. The convective heat exchanged in the air channel can be calculated by the

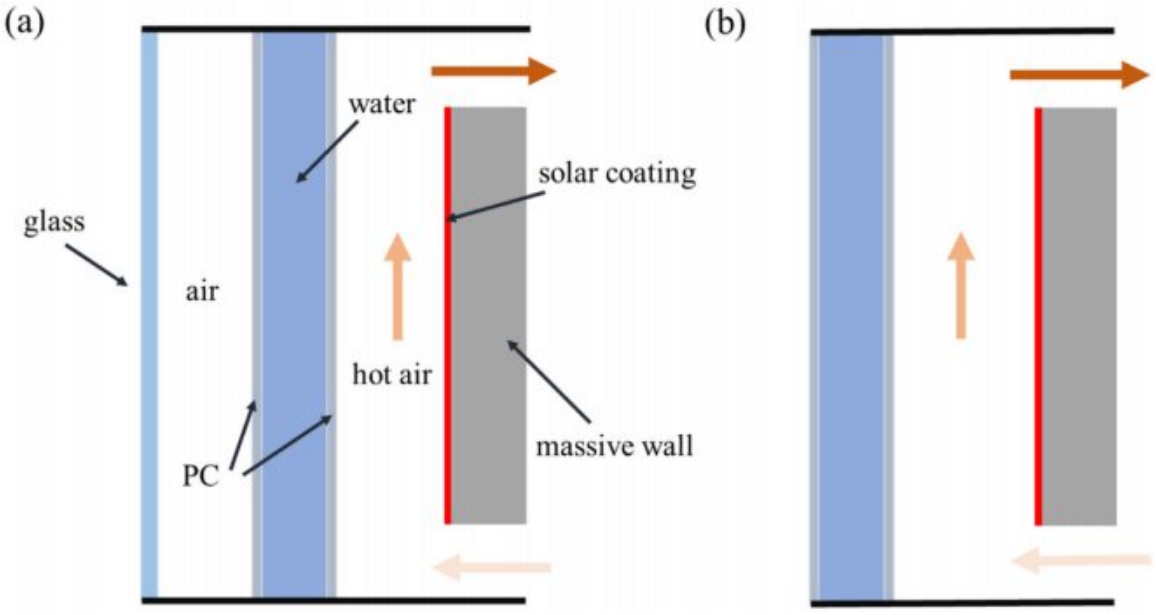

Fig. 1. Two types of composite Trombe walls. (a) Glass–Water Trombe wall, (b) Water Trombe wall.

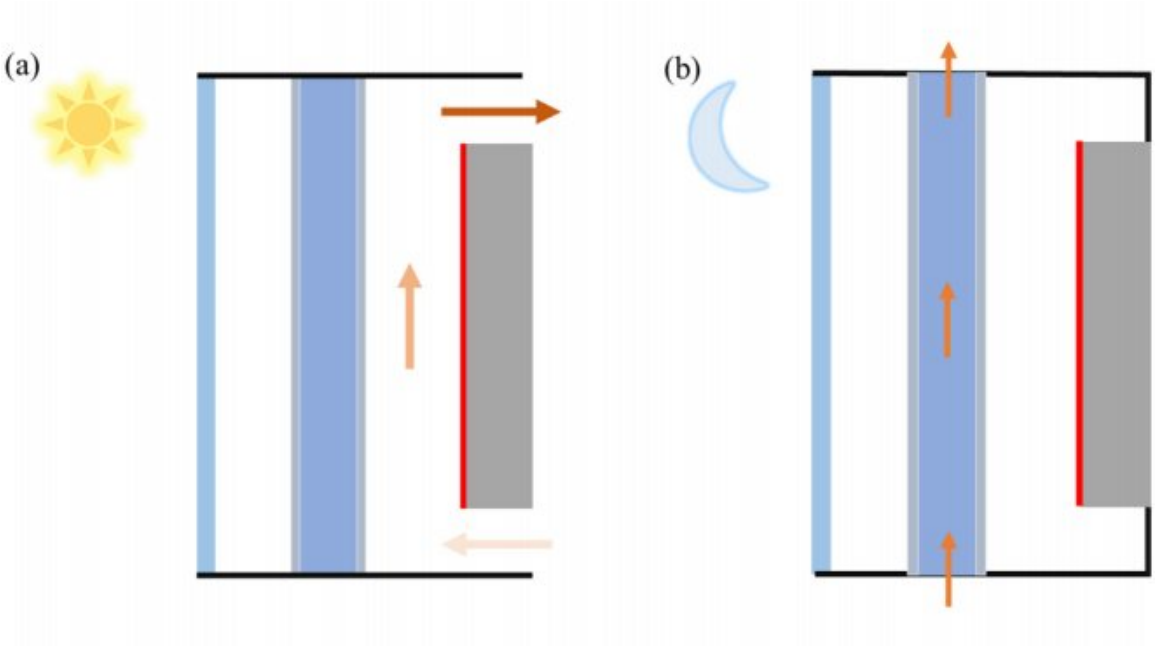

Fig. 2. The operation model of the composite Trombe wall. (a) heat-collecting mode, (b) heat- preservation mode.

Eq. (1) [21].

$$Q_{air} = \dot{m} c_p (\bar{T}_{out} - \bar{T}_{in}) \tag{1}$$

The thermal efficiency of the Trombe wall is defined as the ratio of the output useful energy to the absorbed solar energy. So η can be obtained as following,

$$\eta = \frac{Q_{air}}{I A_{wall}} \tag{2}$$

The exergy balance equation is expressed as following,

$$\dot{E}x_{rad} + \sum \dot{E}x_{in,f} - \sum \dot{E}x_{out,f} - \sum \dot{E}x_{loss} - \sum \dot{E}x_d = 0 \tag{3}$$

where $\dot{E}x_{rad}$ is the exergy of solar radiation,

$$\dot{E}x_{rad} = I \cdot \tau_s = I\left[1 - \frac{4}{3} \cdot \frac{T_a}{T_s} + \frac{1}{3} \cdot \left(1 - \frac{T_a}{T_s}\right)^4\right] \tag{4}$$

$\dot{E}x_{in,f}$ is the exergy of the inlet fluid, $\dot{E}x_{out,f}$ is exergy of the outlet fluid, $\dot{E}x_{loss}$ is the lost exergy, $\dot{E}x_d$ is the total destroyed exergy due to the irreversibility. $\dot{E}x_{gain}$ is given by the exergy balance in the control volume,

$$\dot{E}x_{gain} = \dot{E}x_{out,f} - \dot{E}x_{in,f} = \dot{m} c_p \left(T_{out} - T_{in} - T_a \ln \frac{T_{out}}{T_{in}}\right) - \frac{\dot{m}}{\rho} \Delta p \frac{T_a}{T_m} \tag{5}$$

Table 1
Material physical parameters.

Parts	Material	Density (kg/m^3)	Specific heat (J/kg 0°C)	Thermal conductivity (W/m °C)
cover	glass	2400	800	1.4
PC	polycarbonate	1200	1250	0.2
wall	concrete	1500	1050	0.76
fluid	water	998.2	4182	0.6

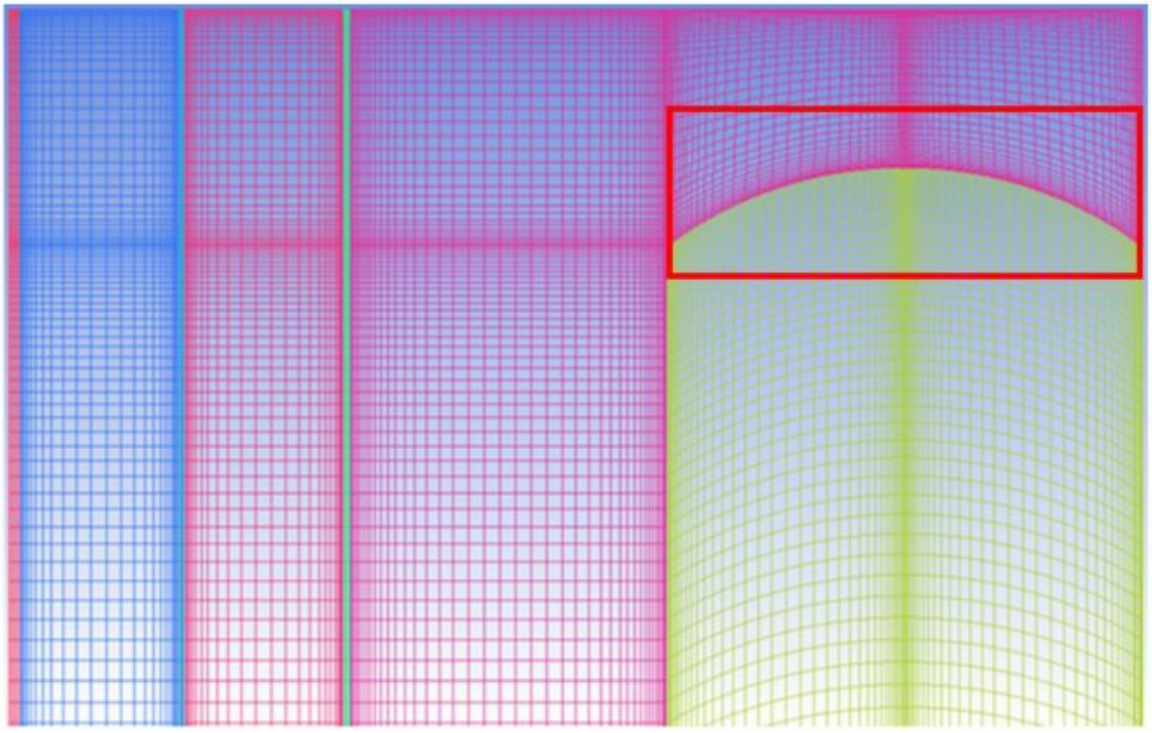

Fig. 3. Part of the grid.

where T_a is the ambient temperature, T_s is the sun temperature of the exergy source which is 75% of the black body temperature of the sun which is approximately around 4350 K [22], Δp is the pressure drop.

The exergy efficiency is defined as the ratio of the gained exergy to the exergy of solar radiation. It is expressed as,

$$\eta_{ex} = \frac{\dot{E}x_{gain}}{\dot{E}x_{rad}} \tag{6}$$

4. Numerical simulation

4.1. Model and meshing

The height of the composite Trombe wall system is 3 m. The thickness of the glass cover is 6 mm, and the transmittance is 89%. The water wall is fixed by two PC boards with a thickness of 12 mm. The spacing between the water wall and the glass cover is 100 mm. The massive wall is made of concrete and the outer surface is painted in black. The wall thickness is 300 mm and the emissivity is 0.9. The spacing between the water wall and massive wall is 100 mm. The upper and lower vents are all 150 mm wide. According to the research results in [23], the massive wall and the underside are all arc-shaped, as shown in the red square in Fig. 3. The physical properties of the materials selected for the composite Trombe wall are shown in Table 1.

The quadrilateral meshes are generated for the whole model, as shown in Fig. 3. The boundary layer grid is refined, which meets the requirement of the turbulence model. The first node spacing is 1 mm to satisfy the $y^+ \leq 1$ condition and the ratio of boundary mesh is 1.2. The grid independence test is conducted and the number of grids is varied from 16,428 to 128,048 in five steps. The grid independence verification selects outlet velocity of the WTW as the reference value. The calculation result indicates that the change of the outlet velocity rate is only 0.51% after 25,296 cells. Hence, the number of grids is 25,296 (124 grids in the x-direction, 204 grids in the y-direction)

4.2. Mathematical model

A two-dimensional model is built to analyze the composite Trombe wall. The Navier–Stokes equations are solved by ANSYS Fluent and these equations are expressed as follows:

Continuity equation,

$$\frac{\partial \rho}{\partial t} + \nabla \cdot (\rho \vec{v}) = 0 \tag{7}$$

Momentum equation,

$$\frac{\partial}{\partial t}(\rho \vec{v}) + \nabla \cdot (\rho \vec{v} \vec{v}) = -\nabla p + \nabla \cdot \left[\mu\left(\nabla \vec{v} + \nabla \vec{v}^T\right)\right] + \rho \vec{g} + \vec{F} \tag{8}$$

Energy equation,

$$\frac{\partial}{\partial t}(\rho E) + \nabla \cdot (\vec{v}(\rho E + p)) = \nabla \cdot \left(k_{eff} \nabla T\right) + S_h \tag{9}$$

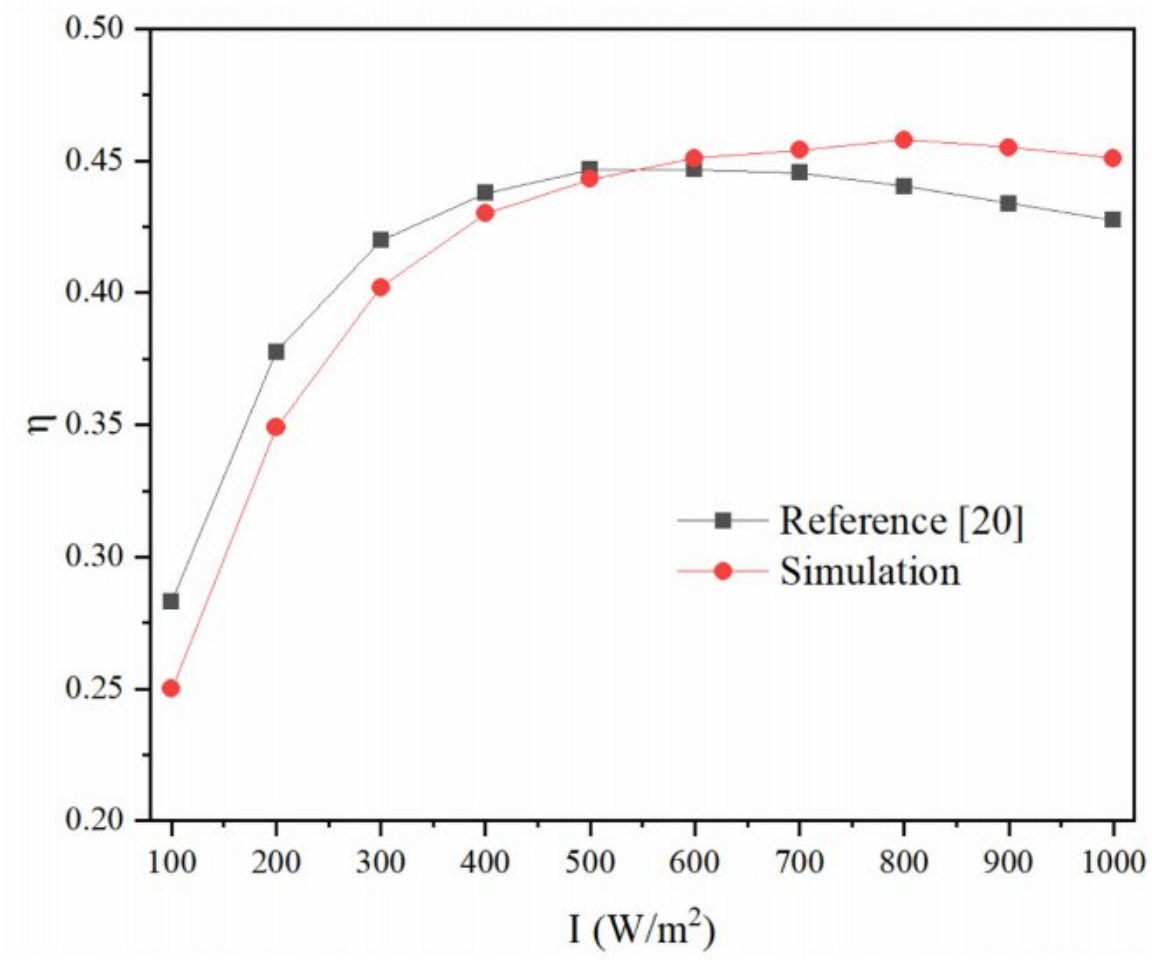

Fig. 4. Comparison of thermal efficiency.

The natural convection simulations of seven turbulence models in a vertical channel with heated wall have been compared [24]. The result indicated that the low-*Re* k-ω model can achieve good accuracy for such problems. Corasanoti et al. [23] conducted a simulation on the Trombe wall and found that the results from the SST k-ω and RSM-stress ω models were closer to the experimental data. The SST k-ω model has good ability to describe characteristics of the buoyance-driven flow. Therefore, the SST k-ω is selected as the turbulence model, and the low-*Re* correction and Enhanced wall function options are enabled in the program. The SST k-ω model comprises two equations [25]. One is k and the other is ω. The equations are defined as follows,

$$\frac{\partial \rho k}{\partial t}+\frac{\partial \rho k u_j}{\partial x_j}=\tilde{P}_k-\rho\beta^* k\omega+\frac{\partial}{\partial x_j}\left[(\mu+\sigma_k\mu_T)\frac{\partial k}{\partial x_j}\right] \tag{10}$$

$$\frac{\partial \rho \omega}{\partial t}+\frac{\partial \rho \omega u_j}{\partial x_j}=\alpha S^2-\rho\beta\omega^2+\frac{\partial}{\partial x_j}\left[(\mu+\sigma_\omega\mu_T)\frac{\partial \omega}{\partial x_j}\right] +2(1-F_1)\sigma_{\omega 2}\frac{1}{\omega}\frac{\partial k}{\partial x_i}\frac{\partial \omega}{\partial x_i} \tag{11}$$

The turbulent viscosity, μ_t is computed as follows,

$$\mu_t=\frac{\rho k}{\omega}\cdot\min\left(\alpha^*,\frac{a_1\omega}{SF_2}\right) \tag{12}$$

where $S=\sqrt{2S_{ij}S_{ij}}$, $\alpha^*=\alpha^*_\infty\left(\frac{\alpha^*_0+\mathrm{Re}_T/R_K}{1+\mathrm{Re}_T/R_K}\right)$, $\mathrm{Re}_T=\frac{\rho k}{\mu\omega}$, $R_k=6$, $\alpha^*_0=0.024$.

The term P_k is the production of turbulence kinetic energy, which can be defined as,

$$P_k=\mu_t\frac{\partial u_i}{\partial x_j}\left(\frac{\partial u_i}{\partial x_j}+\frac{\partial u_j}{\partial x_i}\right) \tag{13}$$

$$\tilde{P}_k=\min(P_k,10\beta^*\rho k\omega) \tag{14}$$

The weighting functions of F_1 and F_2 are calculated by the following formula, respectively,

$$F_1=\tanh\left\{\left\{\min\left[\max\left(\frac{\sqrt{k}}{\beta^*\omega y},\frac{500\nu}{y^2\omega}\right),\frac{4\rho\sigma_{\omega 2}k}{D^+_\omega y^2}\right]\right\}\right\} \tag{15}$$

where $D^+_\omega=\max(2\rho\sigma_{\omega 2}\frac{1}{\omega}\frac{\partial k}{\partial x_i}\frac{\partial \omega}{\partial x_i},10^{-10})$.

$$F_2=\tanh\left\{\left[\max\left(\frac{\sqrt{k}}{\beta^*\omega y},\frac{500\nu}{y^2\omega}\right)^2\right]\right\} \tag{16}$$

In this paper, the discrete ordinates (DO) radiation mode is adopted to solve the radiation problem of the composite Trombe wall. For the composite Trombe wall, it contains semitransparent medium, such as glass and water. However, the semitransparent medium is considered as gray body in general, which may lead to an incorrect consequence. The DO model allows to model semitransparent medium that ensures an accurate simulation result [26]. The *Boussinesq* approach is used to deal with the variation of air density in ANSYS Fluent.

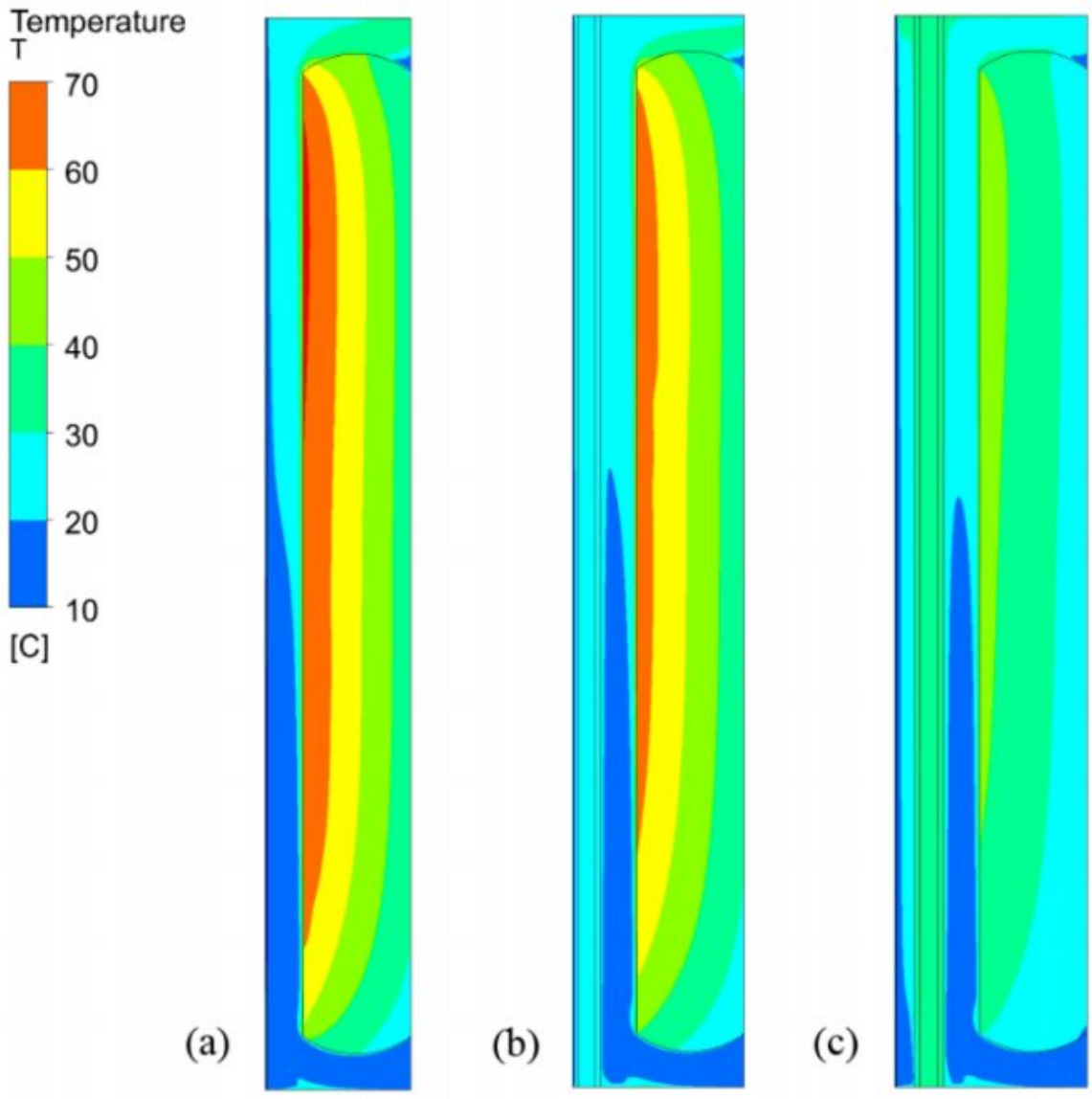

Fig. 5. Temperature fields for the three configurations. (a) TW, (b) WTW, (c) GWTW.

In the present simulation governing equations of continuity, momentum and energy equations are solved by the finite volume method in the steady-state regime. A pressure-based double-precision solver was selected to solve the set of equations with the coupled algorithm. Body Force Weighted scheme was used for pressure discretization. The Second Order Upwind difference scheme is used to discretize the convection and diffusion terms [27].

4.3. Boundary conditions

When the composite Trombe wall is operated at heat-collecting mode, the lower vent is selected as the pressure inlet, the inlet temperature is 15 °C, the upper vent is selected as the pressure outlet, and the backflow temperature is set to 15 °C. In order to make the system be applicate widely, the ambient temperature is set as 0 °C. What's more, cold areas in China are defined as the regions where the averaged air temperature of the coldest month is lower than −3.0 °C. If the composite Trombe wall is effective on the simulated climatic conditions, it could be promoted in cold areas of China. The convective coefficient between the external environment and the cover is 15 W/m^2, and the external radiant temperature is equal to the ambient temperature. The radiation heat transfer between the building envelope and the environment can not be ignored. Therefore, the radiative heat transfer toward the sky and ground is considered as the boundary condition and the external radiation temperature set as the ambient temperature. The top and bottom surfaces are set as adiabatic walls. The convective heat transfer coefficient between the massive wall and the indoor is 5 W/m^2. Assume that the solar radiant flux is 600 W/m^2 and is incident perpendicularly. When operating at night, the ambient temperature is set to −10 °C and the convective heat transfer coefficient of the outer and cover plates is 15 W/m^2. The indoor temperature is 20 °C. The effects of inlet temperature, flow rate and solar radiation intensity on the thermal performance of the composite Trombe wall are investigated. The corresponding simulation variables are shown in Table 2.

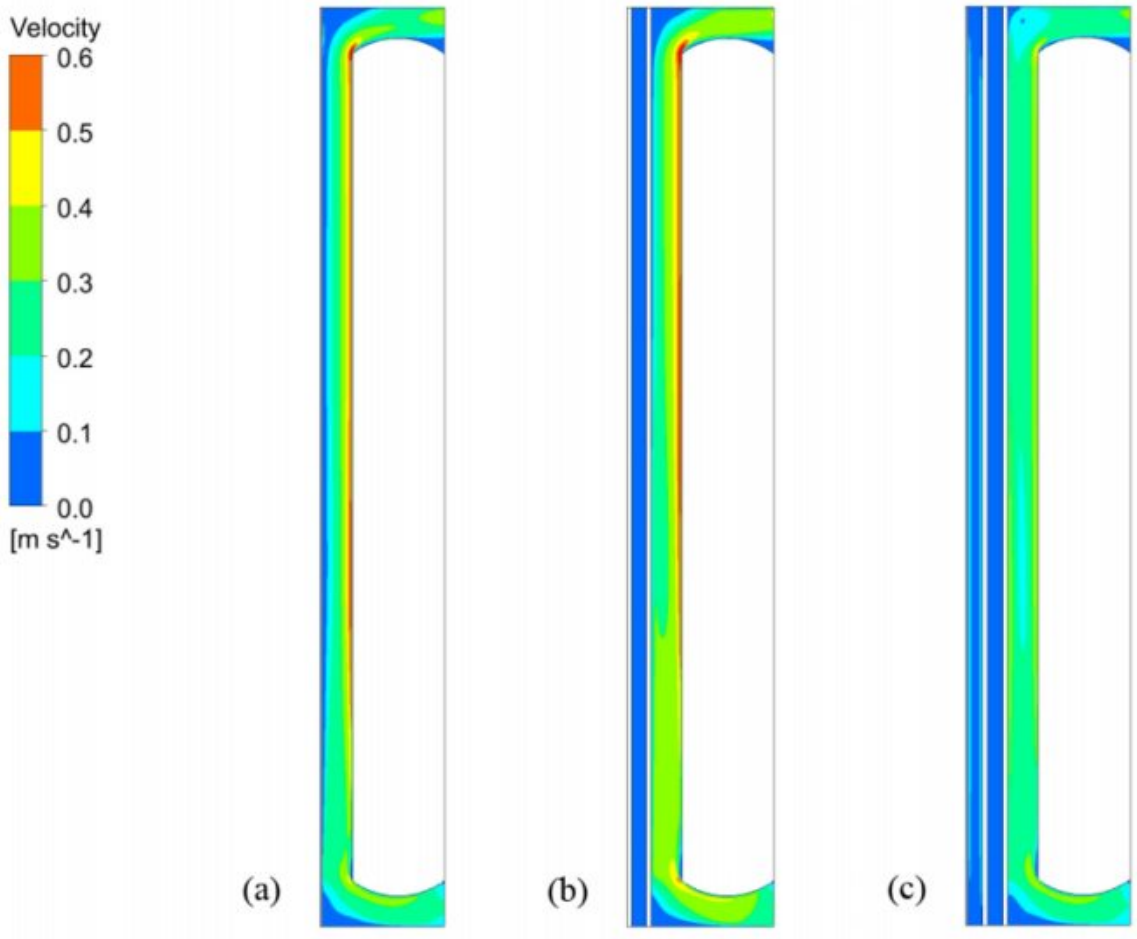

Fig. 6. Velocity fields for the three configurations. (a) TW, (b) WTW, (c) GWTW.

Table 2
Simulation parameters.

Parameters	Values					
Water temperature (°C)	0	2	4	6	8	–
Solar radiation intensity (W/m^2)	300	400	500	600	700	800
Inlet velocity (kg/s)	0.2	0.4	0.6	0.8	0.1	–

Table 3
The comparison of thermal performance for the three configurations.

	TW	WTW	GWTW
T_{out} (°C)	33.1	31.2	28.33
$\dot{m}$ (kg/s)	0.022	0.027	0.021
Q_{air} (W)	393.71	446.06	282.45
$q_{in\text{-}wall}$ (W/m^2)	91.45	82.28	47.66
$\dot{E}x_{gain}$ (W)	32.74	40.28	21.66
η	0.24	0.28	0.17
η_{ex}	0.015	0.022	0.011

5. Results and discussions

5.1. Model verification

To validate the accuracy of the numerical model, the simulated results are compared to the results for a traditional TW from reference [21]. A CFD model is established according to the literature [21]. The comparison of energy efficiencies of the traditional Trombe walls between simulation and data in literature were carried out referring to different solar radiation intensities and shown in Fig. 4. The relative error (*RE*) is selected as evaluation indicator. The *RE* between simulation values and reference results is calculated by:

$$RE = \left| \frac{X_{ref} - X_{sim}}{X_{ref}} \right| \times 100\% \quad (17)$$

The maximum value of *RE* is 10.4%. It could be concluded that the CFD predicted data agrees well with the reference's result.

5.2. Comparison of different Trombe walls

The thermal performance of different Trombe wall at heating mode has been compared under the steady state conditions. The temperature fields of the TW, WTW and GWTW are obtained, as shown in Fig. 5. For the temperature of the heating storage wall, the temperature distribution of TW is the highest and the GWTW is the lowest. It is because the irradiance intensity received by the heat absorbing coating of the TW massive wall is the highest. The introduction of the water wall reduces the incident solar radiation, and the radiation intensity is reduced further for the GWTW due to the glass cover. The temperature in the lower right corner of the upper vent is low because the effect of air backflow. Therefore, when calculating the efficiency, the average temperature of the top of the massive wall's arc to the roof in *y*-direction is used as the outlet temperature. Fig. 6 shows the velocity fields of dif-

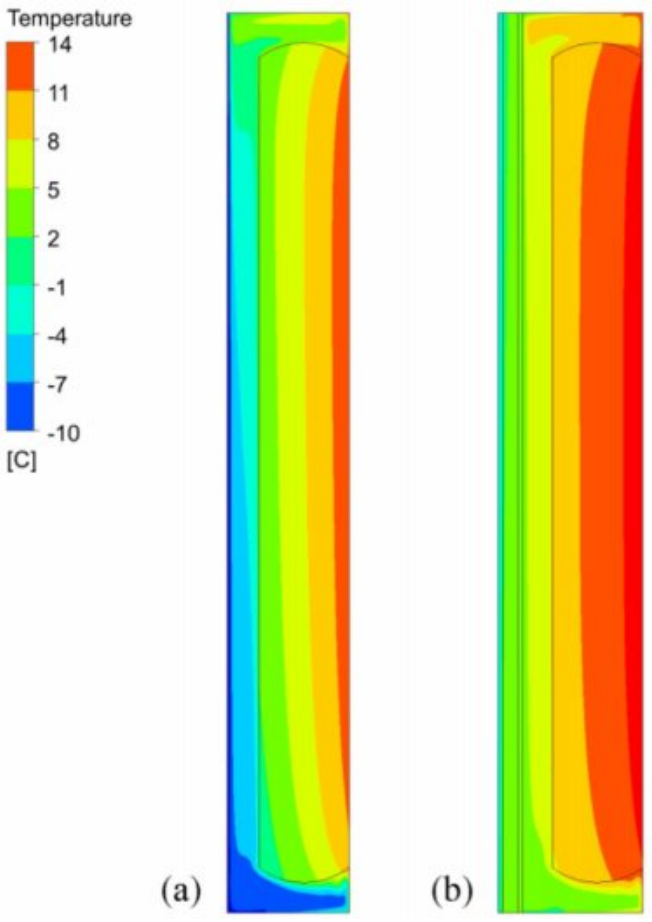

Fig. 7. Temperature distribution for the two configurations. (a) TW, (b) WTW.

ferent Trombe walls. It can be observed that in WTW, the velocity in the flow channel is significantly higher than the other two forms. For the air flow inside the TW, the temperature of the glass cover is always low, so that the heated air shrinks on the side of glass cover which may cause backflow. However, since the temperature of the massive wall is lower than that of the other two types Trombe walls, the density change of the air is small and the air flow is weakened.

The main thermal performance parameters for the three types of Trombe walls are listed in Table 3. Although the TW has the highest outlet temperature, the outlet flow rate is reduced by 19% with respect to WTW, which causes the hot air supplied to the room is reduced. The thermal efficiencies of three Trombe walls are 24%, 28% and 17%, respectively. The difference in thermal efficiency between WTW and GWTW was 11%. Comparing the heat transfer from the massive wall to the room, it can be found that the heat transfer by TW reaches 91.45 W/m^2, while the WTW is 10% lower than the former and the GWTW is 47% lower. Combining the heat transfer of the hot air and the massive wall, it can be found that the WTW is the highest, which can reach 446.06 W/m^2, while the TW is 393.71 W/m^2 and the GWTW is only 282.45 W/m^2. For the exergy gain, the value of WTW is higher than that of the other two types. It can be concluded that the WTW has the best thermal performance. Therefore, the type of GWTW would not be considered in the following chapters.

The temperature fields of the TW and WTW in the nighttime is shown in Fig. 7, where the inlet temperature of the water wall is 4 °C and the mass flow is 0.06 kg/s. It can be observed that the overall temperature of the WTW is significantly higher than that of the TW, indicating that the introduction of the water wall can effectively reduce the heat loss of the building envelope. The heat loss of TW is 35.3 W/m^2 and the WTW is 24.4 W/m^2, which has a decrease of 31%. In summary, the WTW can effectively improve the daytime heat collection performance while reducing nighttime heat loss.

5.3. Influence of irradiance

The efficiency comparison between the TW and WTW at different irradiation intensities is shown in Fig. 8. It can be obtained that the thermal efficiency of WTW is 7.2% higher than the TW, when the solar radiation intensity is 300 W/m^2. As the I increase, the gap of η for the two forms gradually narrows. When I equal to 800 W/m^2, the WTW is 2.6% higher than that of the TW. According to the literature [28], the temperature of TW needs to reach a point before it can operate normally. The thermal performance of WTW under low irradiation can effectively extend its running time.

The exergy comparison of the TW and WTW is presented in Fig. 9 under different irradiation intensity conditions. As the intensity of the irradiation increases, the exergy gain gradually increases and the exergy gain of WTW is larger than that of the TW. The energy efficiencies of the two types of Trombe walls are relatively high, but exergy efficiency is very low. The exergy destruction due to absorption of the absorber plate is the largest [21]. The variation of the exergy efficiency is shown in Fig. 8(b) is similar to the thermal efficiency curve of Fig. 8. Due to the small temperatures involved for Trombe wall system, the absolute values of the exergy efficiency are small.

5.4. Influence of water mass flow rate and inlet temperature

The effect of the water flow rate on the thermal performance of the WTW is shown in Fig. 10, as the temperature of inlet water is 4 °C. When the mass flow rate increases, the heat loss of the WTW is gradually decreasing and tends to be stable. When $\dot{m}$increases from 0.02 kg/s to 0.1 kg/s, the heat loss is reduced by 0.84 W/m^2. When $\dot{m}$ changes from 0.02 kg/s to 0.06 kg/s, the difference in heat loss is 0.7 W/m^2. Accordingly, when the flow rate increases from 0.06 kg/s to 0.1 kg/s, the difference in heat loss is only 0.15 W/m^2. Because of the limitation of water flow rate increase, the water flow rate can be set at 0.06 kg/s to achieve the desired effect. Besides, the continually increasing of the water flow rate will cause the energy consumption of the pump increased.

The effect of the inlet water temperature on the thermal performance of the WTW is shown in Fig. 11, as the mass flow rate is 0.06 kg/s. The inlet water temperature has a linear relation with the heat loss and the Q_{loss} decreases with increasing T_{water}. When T_{water} increases from 0 °C to 8 °C, the Q_{loss} decreases from 27.3 W/m^2 to 21.5 W/m^2.

6. Conclusion

A composite Trombe wall is proposed that combines the water wall with the traditional Trombe wall. The thermal performances of the new designed structures are studied through CFD simulation. From the thermal analysis, the effect of various parameters such as solar radiation intensity, ambient temperature, inlet water flow rate and inlet water temperature on energy efficiency, exergy efficiency and heat loss were analyzed. It is also concluded that the structure has the advantages to directly utilize low-temperature water for reducing building heat loss at nighttime. The main conclusions can be drawn from the study as following:

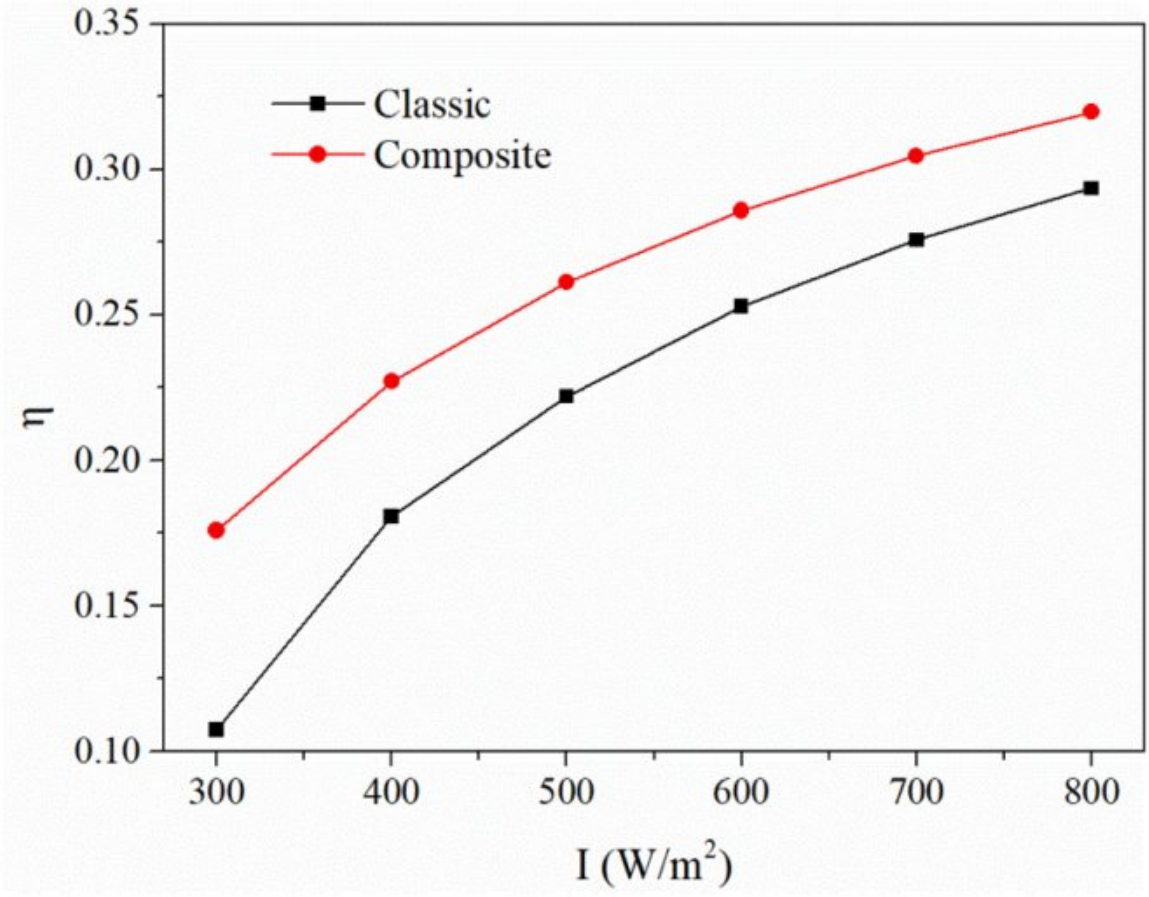

Fig. 8. The effect of different radiation intensities on thermal efficiency.

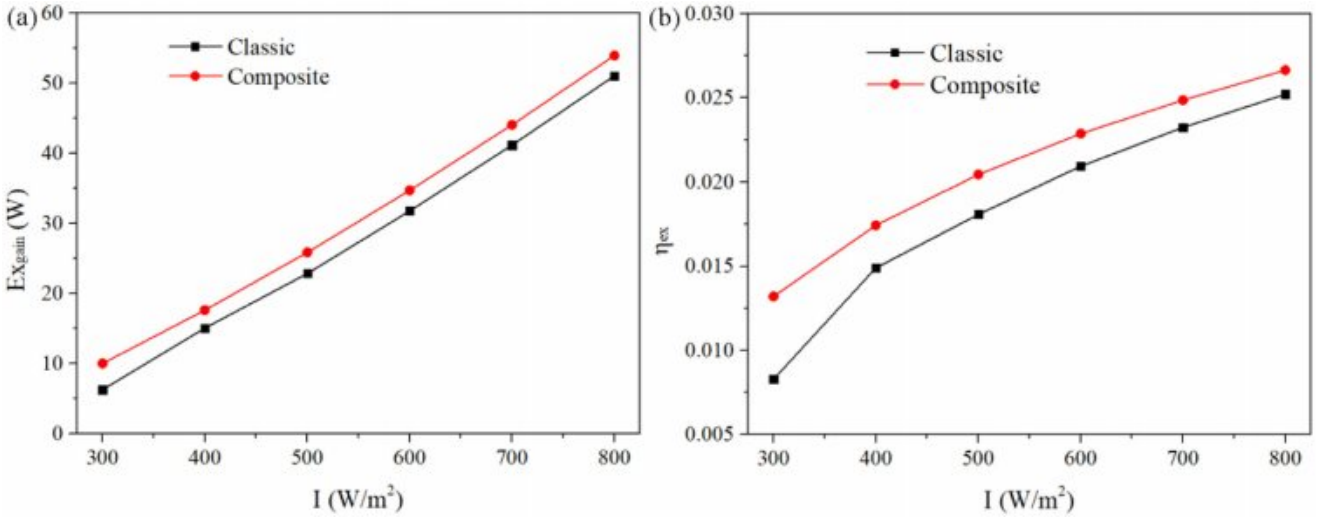

Fig. 9. The exergy analysis for different Trombe walls. (a) exergy gain, (b) exergy efficiency.

(1) The analysis of the TW, WTW and GWTW are carried out respectively on heat-collecting mode. The results indicate that the WTW has the best thermal performance in daytime. This is because that the WTW is able to reduce the natural convection. In the simulated conditions, its efficiency is 3.3% higher than that of the TW. The exergy analysis also indicates that the exergy efficiency of the WTW is highest of the three types;
(2) The thermal efficiency performance of WTW is significantly superior to conventional structures with low irradiance. As the irradiance increases, the gap gradually shrinks, but the efficiency of WTW remains higher than the traditional structure;
(3) The results indicate that the TWT may reduce the external heat transfer significantly by directly using low-temperature water. Comparing the thermal performance of TW and WTW at nighttime, the results show that the WTW can reduce heat loss by 31% comparing to TW.
(4) The mass flow rate of water has minor effect on thermal performance of the WTW. According to the simulation result, the optimal mass flow rate is 0.06 kg/s.

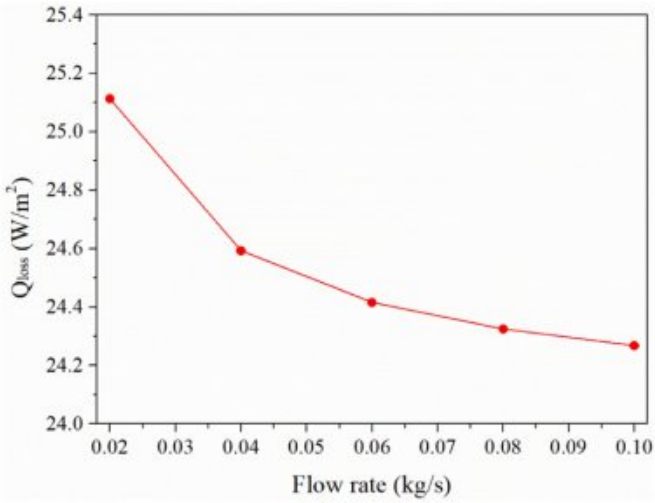

Fig. 10. The effect of flow rate on the WTW.

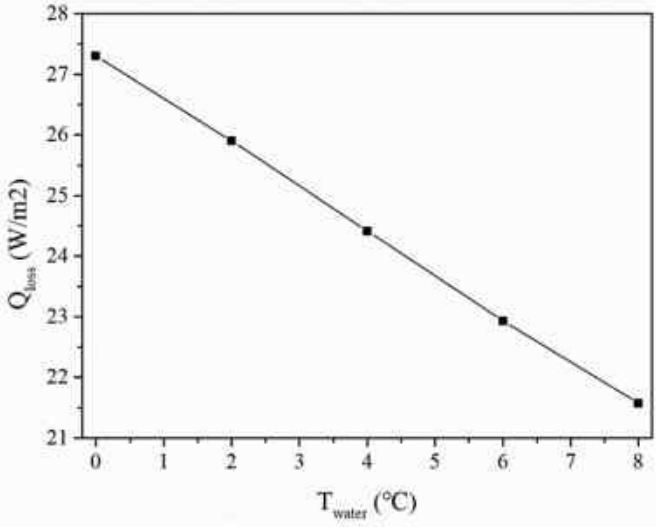

Fig. 11. The effect of T_{water} on the WTW.

Declaration of Competing Interest

We declare that we have no financial and personal relationships with other people or organizations that can inappropriately influence our work, there is no professional or other personal interest of any nature or kind in any product, service and/or company that could be construed as influencing the position presented in, or the review of, the manuscript entitled, "*Investigation on the thermal performance of a composite Trombe wall under steady state condition*".

CRediT authorship contribution statement

Liqun Zhou: Conceptualization, Methodology, Formal analysis, Writing - original draft. **Junpeng Huo:** Methodology, Formal analysis, Writing - original draft. **Tong Zhou:** Conceptualization. **Shufeng Jin:** Supervision.

Acknowledgments

The simulation work completed under cooperation with Lanzhou University of Technology-Ansys Joint Simulation Laboratory, China.

Supplementary materials

Supplementary material associated with this article can be found, in the online version, at doi:10.1016/j.enbuild.2020.109815.

References

[1] K. Yu, Y. Tan, T. Zhang, X. Jin, J. Zhang, X. Wang, Experimental and simulation study on the thermal performance of a novel flue composite wall, Build. Environ. 151 (2019) 126–139.
[2] S.S.S. Baljit, H.-.Y. Chan, K. Sopian, Review of building integrated applications of photovoltaic and solar thermal systems, J. Clean. Prod. 137 (2016) 677–689.
[3] K.H. Kashif Irshad, R. Saidur, M.W. Kareem, Bidyut Baran Saha, Study of thermoelectric and photovoltaic facade system for energy efficient building development: a review, J. Clean. Prod. 2019 (2019) 1376–1395.
[4] Z. Hu, W. He, J. Ji, S. Zhang, A review on the application of Trombe wall system in buildings, Renew. Sustain. Energy Rev. 70 (2017) 976–987.
[5] T. Zhang, Y. Tan, H. Yang, X. Zhang, The application of air layers in building envelopes: a review, Appl. Energy 165 (2016) 707–734.
[6] T. Bajc, M.N. Todorović, J. Svorcan, CFD analyses for passive house with Trombe wall and impact to energy demand, Energy Build. 98 (2015) 39–44.
[7] X. Hong, W. He, Z. Hu, C. Wang, J. Ji, Three-dimensional simulation on the thermal performance of a novel Trombe wall with venetian blind structure, Energy Build. 89 (2015) 32–38.
[8] J. Dong, Z. Chen, L. Zhang, Y. Cheng, S. Sun, J. Jie, Experimental investigation on the heating performance of a novel designed trombe wall, Energy 168 (2019) 728–736.
[9] F. Abbassi, L. Dehmani, Experimental and numerical study on thermal performance of an unvented Trombe wall associated with internal thermal fins, Energy Build. 105 (2015) 119–128.
[10] B. Kundakci Koyunbaba, Z. Yilmaz, The comparison of Trombe wall systems with single glass, double glass and PV panels, Renew. Energy 45 (2012) 111–118.
[11] O. Saadatian, K. Sopian, C.H. Lim, N. Asim, M.Y. Sulaiman, Trombe walls: a review of opportunities and challenges in research and development, Renew. Sustain. Energy Rev. 16 (2012) 6340–6351.
[12] Y.A. Kara, A. Kurnuç, Performance of coupled novel triple glass and phase change material wall in the heating season: an experimental study, Solar Energy 86 (2012) 2432–2442.
[13] X. Liu, Y. Zhou, G. Zhang, Numerical study on cooling performance of a ventilated Trombe wall with phase change materials, Build. Simul. 11 (2018) 677–694.
[14] W. Sun, J. Ji, C. Luo, W. He, Performance of PV-Trombe wall in winter correlated with south façade design, Appl. Energy 88 (2011) 224–231.
[15] Z. Hu, W. He, D. Hu, S. Lv, L. Wang, J. Ji, et al., Design, construction and performance testing of a PV blind-integrated Trombe wall module, Appl. Energy 203 (2017) 643–656.
[16] T. Wu, C. Lei, A review of research and development on water wall for building applications, Energy Build. 112 (2016) 198–208.
[17] H. Wang, C. Lei, Theoretical modeling of combined solar chimney and water wall for buildings, Energy Build. 187 (2019) 186–200.
[18] T. Wu, C. Lei, CFD simulation of the thermal performance of an opaque water wall system for Australian climate, Solar Energy 133 (2016) 141–154.
[19] C. Shen, X. Li, S. Yan, Numerical study on energy efficiency and economy of a pipe-embedded glass envelope directly utilizing ground-source water for heating in diverse climates, Energy Convers. Manag. 150 (2017) 878–889.
[20] Y. Yu, F. Niu, H.-.A. Guo, D. Woradechjumroen, A thermo-activated wall for load reduction and supplementary cooling with free to low-cost thermal water, Energy 99 (2016) 250–265.
[21] S. Duan, C. Jing, Z. Zhao, Energy and exergy analysis of different Trombe walls, Energy Build. 126 (2016) 517–523.
[22] D.G. Gunjo, P. Mahanta, P.S. Robi, Exergy and energy analysis of a novel type solar collector under steady state condition: experimental and cfd analysis, Renew. Energy 114 (2017) 655–669.
[23] S. Corasaniti, L. Manni, F. Russo, F. Gori, Numerical simulation of modified Trombe-Michel Walls with exergy and energy analysis, Int. Commun. Heat Mass Trans. 88 (2017) 269–276.
[24] M. Abdollahzadeh, M. Esmaeilpour, R. Vizinho, A. Younesi, J.C. Pàscoa, Assessment of RANS turbulence models for numerical study of laminar-turbulent transition in convection heat transfer, Int. J. Heat Mass Transf. 115 (2017) 1288–1308.
[25] P.A.C. Rocha, H.H.B. Rocha, F.O.M. Carneiro, M.E. Vieira da Silva, A.V. Bueno, k–ω SST (shear stress transport) turbulence model calibration: a case study on a small scale horizontal axis wind turbine, Energy 65 (2014) 412–418.
[26] L. Zhou, Y. Wang, Q. Huang, Parametric analysis on the performance of flat plate collector with transparent insulation material, Energy 174 (2019) 534–542.
[27] , ANSYS. ANSYS Fluent Theory Guide, ANSYS Inc, USA, 2015.
[28] B. Zamora, A.S. Kaiser, Influence of the shape, thermal radiation, and variable properties on the turbulent buoyancy-driven airflow inside cavities with Trombe wall geometry, Numer. Heat Trans., Part A 73 (2018) 307–331.